J. Meas. Sci. Instrum., 2024, 15(4): 445-457. http://jmsi.publish.founderss.cn/
DOI: 10.62756/jmsi.1674-8042.2024045 jmsi@nuc.edu.cn

A stepwise camera calibration method incorporating compensation for eccentricity error

WEI Jiaqi, WANG Peng*, LI Yue, LI Mojing, LI Lin, SUN Changku, FU Luhua

State Key Laboratory of Precision Measurement Technology and Instruments, Tianjin University, Tianjin 300072, China

***Corresponding author:** WANG Peng (wang_peng@tju.edu.cn)

Received: September 29, 2024 **Revised:** November 11, 2024 **Accepted:** December 7, 2024

Abstract: In visual measurement, high-precision camera calibration often employs circular targets. To address issues in mainstream methods, such as the eccentricity error of the circle from using the circle's center for calibration, overfitting or local minimum from full-parameter optimization, and calibration errors due to neglecting the center of distortion, a stepwise camera calibration method incorporating compensation for eccentricity error was proposed to enhance monocular camera calibration precision. Initially, the multi-image distortion correction method calculated the common center of distortion and coefficients, improving precision, stability, and efficiency compared to single-image distortion correction methods. Subsequently, the projection point of the circle's center was compared with the center of the contour's projection to iteratively correct the eccentricity error, leading to more precise and stable calibration. Finally, nonlinear optimization refined the calibration parameters to minimize reprojection error and boosts precision. These processes achieved stepwise camera calibration, which enhanced robustness. In addition, the module comparison experiment showed that both the eccentricity error compensation and the camera parameter optimization could improve the calibration precision, but the latter had a greater impact. The combined use of the two methods further improved the precision and stability. Simulations and experiments confirmed that the proposed method achieved high precision, stability, and robustness, suitable for high-precision visual measurements.

Key words: camera calibration; error compensation; eccentricity error; distortion correction; center of distortion; optical measurement

0 Introduction

Camera calibration plays a crucial role in visual measurement and three-dimensional reconstruction, as its precision directly affects the final measurement outcomes. Consequently, research on high-precision and noise-resistant camera calibration methods continues to be a primary focus[1-3]. Camera calibration methods are generally categorized into three types: target calibration methods[4,5], self-calibration methods[6,7], and hybrid calibration methods[8,9]. Among these, 2D pattern-based target calibration methods are widely used in industrial visual measurements due to their high precision, robustness, and cost-effectiveness. Zhang's chessboard-based calibration method[10] is the most representative of these methods. It involves capturing multiple images of the target from various positions to compute camera parameters based on the correspondence of corner points. Nonlinear techniques are subsequently employed to estimate lens distortion parameters, followed by the optimization of all parameters. However, the detection of chessboard corners can be significantly influenced by noise. Subsequent research has utilized circular targets in place of chessboards, as the detection of arc centers provides greater precision and better resistance to interference[11,12]. However, when the calibration target plane is not parallel to the imaging plane, the circular profile is projected as an ellipse due to perspective distortion. Consequently, the projection of the circle's center does not align with the center of the ellipse. Using the center of the ellipse as the projected center of the circle for camera calibration leads to errors. To ensure calibration precision, it is essential to mitigate the impact of the eccentricity error of the circle[13].

To mitigate calibration errors resulting from the eccentricity error of the circle, two primary methods are employed. One method is to directly determine the center of the true circle projection by adding constraints. Yu et al.[14] used encoded concentric rings on a liquid crystal display (LCD) to directly determine the coordinates of the circle's center. However, it does not address the reflection issue of the LCD, which may lead to errors in point extraction. Wen et al.[15] combined complete and incomplete

concentric circles, employing photogrammetric techniques to obtain the true projection point of the circle's center and eliminate the eccentricity error. However, this method requires specially designed irregular targets and is costly. Liang et al.[16] used the conjugate polar properties of two coplanar circles to compute the vanishing line and then performed camera calibration based on the relationship between the circle's center and the imaging absolute cone. However, this method has lower precision. Another method involves iteratively compensating for the eccentricity error. Datta et al.[11] introduced regular planar surfaces to compensate the eccentricity error and iteratively computed camera parameters. However, this method is prone to local minima. Lin et al.[17] employed a two-step method, starting with coarse calibration, then aligning the ellipse plane with the target plane, locating the circle center, and mapping it back for iterative computation. This method is significantly affected by the results of coarse calibration, leading to instability and local minima. Shen et al. [18] examined the impact of lens distortion on the eccentricity error and developed a compensation framework that iteratively optimized the projection point of the true circle center. However, this method simultaneously optimizes all parameters, which may lead to calibration errors due to parameter inaccuracies, overfitting, or local optima.

Generally, the second category of methods offers better calibration precision due to the use of nonlinear optimization and iterative algorithms. However, these methods often treat the principal point (PP) as the center of distortion (CoD) and optimize all camera and distortion parameters together, which can cause overfitting among parameters. Therefore, separating the calibration of distortion parameters from camera parameters can further enhance both precision and robustness.

In visual measurement, lens distortion inevitably occurs with wide-angle lenses due to manufacturing defects or misalignment of optical components. Typically, the PP does not align with the CoD[19,20]. Consequently, correcting distortion with respect to the CoD has become a prominent focus in camera calibration research. Stepwise methods for camera calibration are of significant research interest. Lens distortion correction algorithms are currently categorized into metric and non-metric methods. Metric methods estimate calibration parameters using predefined calibration objects. Hartley et al. [21] calculated the CoD in a non-parametric form and then determined other calibration parameters linearly using multiple image sets. However, this method has relatively low precision. Hong et al. [22] derived the CoD using Hartley's method and employed point correspondences to determine distortion parameters and the homography matrix, requiring at least three images to decompose the camera parameters. Although this method is efficient, it does not account for the joint estimation of distortion parameters across multiple images which can improve calibration precision.

Non-metric methods, however, do not rely on known reference objects or relationships. Instead, they employ projection geometry invariants, such as cross-ratios, linearity, vanishing points, and plane constraints, to stepwise calibrate distortion coefficients and camera parameters. Sun et al.[23] optimized distortion parameters using geometric constraints from vanishing points and linearity, followed by the linear estimation of camera parameters. However, the vanishing points were derived from an initial homography matrix, impacting the initial calibration results. Dang et al. [24] introduced additional constraints for distortion correction by defining a distortion measurement function based on coplanar vanishing points, weighted linearity errors, and cross-ratio invariance. They performs nonlinear optimization to estimate distortion parameters and then determines camera parameters through linear methods. However, the study does not provide a method for computing initial distortion parameters. Consequently, the results of nonlinear optimization are heavily dependent on initial values, rendering them vulnerable to local minima. These methods use either checkerboard patterns or circular targets for calibration but do not account for the eccentricity error of the circle. Therefore, improvements in camera calibration methods are required to enhance precision.

As discussed earlier, the compensation for the eccentricity error of the circle is seldom addressed in stepwise camera calibration methods. A stepwise camera calibration method was proposed that included compensation for the eccentricity error. This method first calculated a common CoD for multiple images based on the correspondence between the centers of circle points and image points. Subsequently, it optimized the radial distortion fundamental matrix by jointly solving for distortion coefficients and the homography matrix. The difference between the projected center of the circle and the projected center of the circle's contour was used as the eccentricity error, which compensated for the centers of circle points in the image. This process was iteratively repeated to optimize the camera's distortion parameters and mitigate the impact of eccentricity error on lens distortion correction. Finally, distortion correction was applied to the elliptical contour points in the image. The ellipse center was fitted using the least squares method and compared to the

ideal center of the target circle's projected contour to assess reprojection error. The Levenberg-Marquardt (L-M) algorithm was then employed for further optimization of camera parameters, ultimately achieving stepwise calibration of distortion and camera parameters. Extensive computer simulations and practical experiments demonstrated that the proposed method provided high precision and robustness, making it suitable for precision-demanding visual measurement applications.

1 Camera model

1.1 Pinhole camera model

The pinhole camera model is illustrated in Fig.1.

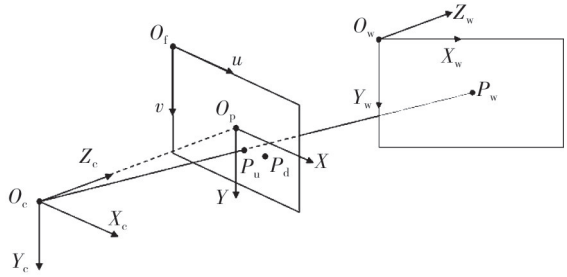

Fig. 1 Mathematical model of camera

Here, $O_cX_cY_cZ_c$ represents the 3D camera coordinate system, O_fuv denotes the 2D pixel coordinate system, O_pXY is the 2D image coordinate system, and $O_wX_wY_wZ_w$ indicates the 3D world coordinate system. During camera calibration, the target plane is typically set to $Z_w=0$, so the homogeneous coordinate of feature points on the target is denoted as $\boldsymbol{P}_w(X_w, Y_w, 1)^T$. After undistorted perspective projection, the homogeneous coordinate is $\boldsymbol{P}_u(u, v, 1)^T$. The relationship between the coordinate is given by

$$\rho\begin{bmatrix}u\\v\\1\end{bmatrix}=\boldsymbol{A}\begin{bmatrix}r_1 & r_2 & r_3 & t\end{bmatrix}=\boldsymbol{A}\begin{bmatrix}r_1 & r_2 & t\end{bmatrix}\begin{bmatrix}X_w\\Y_w\\1\end{bmatrix},$$

$$\text{with } \boldsymbol{A}=\begin{bmatrix}f_x & 0 & u_0\\0 & f_y & v_0\\0 & 0 & 1\end{bmatrix}, \tag{1}$$

where ρ is an arbitrary scaling factor; $\boldsymbol{A}$ is the camera intrinsic matrix, with f_x and f_y the focal lengths in pixels, (u_0, v_0) the coordinates of the principal point; r_i denotes the ith column of the rotation matrix $\boldsymbol{R}$, and t is the translation vector $\boldsymbol{T}$. The relationship between world points and their images can be expressed as

$$\rho\boldsymbol{P}_u=\boldsymbol{H}\boldsymbol{P}_w, \text{ with } \boldsymbol{H}=\boldsymbol{A}\begin{bmatrix}r_1 & r_2 & t\end{bmatrix}. \tag{2}$$

1.2 Lens distortion model

Lens manufacturing often results in lens distortion, necessitating the use of an appropriate distortion model for precise camera imaging. The most widely used model is the polynomial model[25], which employs two radial distortion parameters and two tangential distortion parameters. However, the latter has minimal impact on measurement results and can be negligible. Therefore, this paper utilizes the radial distortion segmentation model (DM)[26], shown as

$$\boldsymbol{P}_u-\boldsymbol{O}_d=\frac{\boldsymbol{P}_d-\boldsymbol{O}_d}{1+\lambda_1 r_d^2+\lambda_2 r_d^4+\cdots}, \tag{3}$$

where $\boldsymbol{O}_d=(du_0, dv_0, 1)^T$ represents the homogeneous coordinates of the CoD (du_0 and dv_0 represent single symbols); λ_1 and λ_2 are the distortion coefficients; $\boldsymbol{P}_d$ is the homogeneous coordinate on an image with distortion, and r_d denotes the distance from $\boldsymbol{P}_u$ to $\boldsymbol{O}_d$.

2 Camera calibration method

2.1 Multi-image distortion correction

A multi-image distortion correction method was proposed based on the methods of Hartley[21] and Hong[22]. The method first solves for the common CoD across all images using point correspondences. It then utilizes the derived linear equations to determine $\hat{F}_{r(i)}$ and subsequently calculates the mean coefficients and homography matrix to complete the multi-image distortion correction. This method facilitates joint correction for multiple images, with the linear solving method ensuring high computational efficiency. The principle of this method is briefly described as follows.

Assuming m calibration images, each image has n feature points. For the jth point in the ith image, multiply both sides of Eq. (3) by $[\boldsymbol{O}_d]_\times$ (the anti-symmetric matrix of $\boldsymbol{O}_d$) and substitute Eq. (2) to get

$$\boldsymbol{P}_{d(i,j)}^T\boldsymbol{F}_{r(i)}\boldsymbol{P}_{w(i,j)}=0, \text{ with } \boldsymbol{F}_{r(i)}=[\boldsymbol{O}_d]_\times\boldsymbol{H}_{(i)}. \tag{4}$$

For all $\boldsymbol{F}_{r(i)}$, the common left epipole is determined as the coordinates $\boldsymbol{O}_d$ of the common CoD. Next, the homography matrix and distortion coefficients are computed with the $\boldsymbol{O}_d$ considered as the origin of the coordinate system, i.e., $\hat{\boldsymbol{O}}_d=(0,0,1)^T$. The transformation matrices before and after the coordinate system change can be expressed as $\boldsymbol{T}=\begin{bmatrix}1 & 0 & -du_0\\0 & 1 & -dv_0\\0 & 0 & 1\end{bmatrix}^T$. It can be obtained that

$$\hat{\boldsymbol{P}}_{d(i,j)}^T\hat{\boldsymbol{F}}_{r(i)}\boldsymbol{P}_{w(i,j)}=0, \text{ with } \hat{\boldsymbol{P}}_{d(i,j)}=\boldsymbol{T}\boldsymbol{P}_{d(i,j)}. \tag{5}$$

Furthermore, $\hat{\boldsymbol{F}}_{r(i)}$ can be expressed as

$$\hat{\boldsymbol{F}}_{r(i)}=[\hat{\boldsymbol{O}}_d]_\times\hat{\boldsymbol{H}}_{(i)}=\begin{bmatrix}0 & -1 & 0\\1 & 0 & 0\\0 & 0 & 0\end{bmatrix}\hat{\boldsymbol{H}}_{(i)}. \tag{6}$$

Let $\hat{\boldsymbol{F}}_{\mathrm{r}(i)}=\left[\hat{\boldsymbol{f}}_{1(i)}^{\mathrm{T}};\hat{\boldsymbol{f}}_{2(i)}^{\mathrm{T}};\hat{\boldsymbol{f}}_{3(i)}^{\mathrm{T}}\right]$, $\widehat{\boldsymbol{H}}_{(i)}=\left[\hat{\boldsymbol{h}}_{1(i)}^{\mathrm{T}};\hat{\boldsymbol{h}}_{2(i)}^{\mathrm{T}};\hat{\boldsymbol{h}}_{3(i)}^{\mathrm{T}}\right]$. The last row of $\hat{\boldsymbol{F}}_{\mathrm{r}(i)}$ is zero, hence Eq. (5) can be simplified to

$$\begin{bmatrix}\hat{x}_{\mathrm{d}(i,j)} & \hat{y}_{\mathrm{d}(i,j)}\end{bmatrix}\begin{bmatrix}\hat{\boldsymbol{f}}_{1(i)}^{\mathrm{T}}\\ \hat{\boldsymbol{f}}_{2(i)}^{\mathrm{T}}\end{bmatrix}\begin{bmatrix}x_{\mathrm{w}(i,j)}\\ y_{\mathrm{w}(i,j)}\\ 1\end{bmatrix}=0. \tag{7}$$

The matrix $\hat{\boldsymbol{F}}_{\mathrm{r}(i)}$ can be obtained through linear decomposition. It can be obtained that

$$\hat{\boldsymbol{h}}_{1(i)}^{\mathrm{T}}=\hat{\boldsymbol{f}}_{2(i)}^{\mathrm{T}},\ \hat{\boldsymbol{h}}_{2(i)}^{\mathrm{T}}=-\hat{\boldsymbol{f}}_{1(i)}^{\mathrm{T}}. \tag{8}$$

After the coordinate system transformation, Eq. (2) becomes

$$\rho_{(i,j)}\hat{\boldsymbol{P}}_{\mathrm{u}(i,j)}=\hat{\boldsymbol{H}}_{(i)}\boldsymbol{P}_{\mathrm{w}(i,j)}. \tag{9}$$

Incorporating the DM distortion model, it can be written as

$$\rho_{(i,j)}\begin{bmatrix}\dfrac{\hat{x}_{\mathrm{d}(i,j)}}{1+\lambda_{1(i)}\hat{r}_{\mathrm{d}(i,j)}^2+\lambda_{2(i)}\hat{r}_{\mathrm{d}(i,j)}^4}\\ \dfrac{\hat{y}_{\mathrm{d(i,j)}}}{1+\lambda_{1(i)}\hat{r}_{\mathrm{d}(i,j)}^2+\lambda_{2(i)}\hat{r}_{\mathrm{d}(i,j)}^4}\\ 1\end{bmatrix}=\begin{bmatrix}\hat{\boldsymbol{h}}_{1(i)}^{\mathrm{T}}\\ \hat{\boldsymbol{h}}_{2(i)}^{\mathrm{T}}\\ \hat{\boldsymbol{h}}_{3(i)}^{\mathrm{T}}\end{bmatrix}\boldsymbol{P}_{\mathrm{w}(i,j)}. \tag{10}$$

To eliminate the scale factor $\rho_{(i,j)}$, the Eq. (10) can be simplified to

$$\begin{bmatrix}\hat{X}_{\mathrm{d}(i,j)}\boldsymbol{P}_{\mathrm{w}(i,j)}^{\mathrm{T}} & -\hat{\boldsymbol{f}}_{2(i)}^{\mathrm{T}}\boldsymbol{P}_{\mathrm{w}(i,j)}\hat{r}_{\mathrm{d}(i,j)}^2 & -\hat{\boldsymbol{f}}_{2(i)}^{\mathrm{T}}\boldsymbol{P}_{\mathrm{w}(i,j)}\hat{r}_{\mathrm{d}(i,j)}^4\\ \hat{y}_{\mathrm{d}(i,j)}\boldsymbol{P}_{\mathrm{w}(i,j)}^{\mathrm{T}} & \hat{\boldsymbol{f}}_{1(i)}^{\mathrm{T}}\boldsymbol{P}_{\mathrm{w}(i,j)}\hat{r}_{\mathrm{d}(i,j)}^2 & \hat{\boldsymbol{f}}_{1(i)}^{\mathrm{T}}\boldsymbol{P}_{\mathrm{w}(i,j)}\hat{r}_{\mathrm{d}(i,j)}^4\end{bmatrix}\cdot\begin{bmatrix}\hat{\boldsymbol{h}}_{3(i)}\\ \lambda_{1(i)}\\ \lambda_{2(i)}\end{bmatrix}=\begin{bmatrix}\hat{\boldsymbol{f}}_{2(i)}^{\mathrm{T}}\boldsymbol{P}_{\mathrm{w}(i,j)}\\ -\hat{\boldsymbol{f}}_{1(i)}^{\mathrm{T}}\boldsymbol{P}_{\mathrm{w}(i,j)}\end{bmatrix}. \tag{11}$$

By using two distortion coefficients, each image requires at least three points to solve Eq. (11) for $\hat{\boldsymbol{h}}_{3(i)}$ and distortion coefficients $\lambda_{1(i)}$ and $\lambda_{2(i)}$. After obtaining $\hat{\boldsymbol{H}}_{(i)}$, the homography matrix for the original image coordinate system $\boldsymbol{H}_{(i)}$ is calculated by

$$\boldsymbol{H}_{(i)}=\boldsymbol{T}^{-1}\hat{\boldsymbol{H}}_{(i)}=\begin{bmatrix}1 & 0 & du_0\\ 0 & 1 & dv_0\\ 0 & 0 & 1\end{bmatrix}\hat{\boldsymbol{H}}_{(i)}. \tag{12}$$

This process yields the homography matrix $\boldsymbol{H}_{(i)}$ and distortion coefficients $\lambda_{1(i)}$ and $\lambda_{2(i)}$. The average distortion coefficients $\bar{\lambda}_1$ and $\bar{\lambda}_2$ are used as the common distortion coefficients λ_1 and λ_2, ultimately achieving linear distortion correction across multiple images.

2.2 Iterative compensation for eccentricity error of circle

The eccentricity error of the circle is defined, as illustrated in Fig. 2. The difference between the circle's projection center $\boldsymbol{P}_{\mathrm{COPD}}$ (Represented by the red part) and the circle contour's projection center $\boldsymbol{P}_{\mathrm{CPDO}}$ (Represented by the blue part) is used as the compensation value δ. The dashed lines represent the stepwise discretization method, where a set of contour points from the model circle is uniformly selected. The projection points of these contour points on the distorted image are calculated, and the center of these projection points is fitted to determine $\boldsymbol{P}_{\mathrm{CPDO}}$.

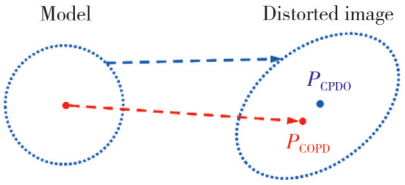

Fig. 2 Illustration of eccentricity error of circle

For a given extracted circle center feature point $\boldsymbol{P}_{\mathrm{d}(i,j)}$, the eccentricity error compensation value is $\delta_{(i,j)}$, and the compensated coordinates of the point are denoted as $\boldsymbol{P}_{\mathrm{dc}(i,j)}$, given by

$$\begin{cases}x_{\mathrm{dc}(i,j)}=x_{\mathrm{d}(i,j)}+\delta_{\mathrm{x}(i,j)},\\ y_{\mathrm{dc}(i,j)}=y_{\mathrm{d}(i,j)}+\delta_{\mathrm{y}(i,j)}.\end{cases} \tag{13}$$

Using the multi-image distortion correction method, the initial values of $\boldsymbol{O}_{\mathrm{d}}{}^{(0)}$, $\bar{\lambda}_1^{(0)}$, $\bar{\lambda}_2^{(0)}$, and $\boldsymbol{H}_{(i)}^{(0)}$ are computed. The eccentricity error of the circle, $\delta_{(i,j)}$, is then corrected using Eqs. (2), (3), and (13). The compensated point $\boldsymbol{P}_{\mathrm{dc}(i,j)}$ is subsequently re-corrected for distortion. Repeatedly iterate the above process until one of the following conditions is satisfied. k is the iteration count and $k>0$. RMS denotes the root mean square value of a set of numbers. $\mathrm{Threshold}_1$ represents the change value of the deviation of the center of the circle, and the empirical value is 0.001 pixel. $\mathrm{Threshold}_2$ represents the change value of the distance of the distortion center coordinates, and the empirical value is 0.05 pixel. The optimal $\boldsymbol{O}_{\mathrm{d}}$, λ_1, λ_2, and $\boldsymbol{H}_{(i)}$ are thus obtained.

$$\text{Cond.1:}\begin{cases}\left\|\mathrm{RMS}\left(\delta_{(i,j)}^{(k)}\right)-\mathrm{RMS}\left(\delta_{(i,j)}^{(k-1)}\right)\right\|<\mathrm{Threshold}_1,\\ \left\|\boldsymbol{O}_{\mathrm{d}}{}^{(k)}-\boldsymbol{O}_{\mathrm{d}}{}^{(k-1)}\right\|<\mathrm{Threshold}_2,\end{cases}$$

$$\text{Cond.2: } k>\mathrm{MaxIters}.$$

2.3 Nonlinear optimization of camera parameters

To compensate for the eccentricity error of the circle, a new reprojection error is defined, as illustrated in Fig. 3. The dashed line represents the discretized solution method. Distortion correction is applied to the extracted elliptical contour points, and the corrected ellipse's center is denoted as P_{EUO} (Represented by the red part).

The equation of the circular model is $(x-\alpha)^2+(y-\beta)^2=\gamma^2$, which can be written as $\boldsymbol{C}=$

$\begin{bmatrix} 1 & 0 & -\alpha \\ 0 & 1 & -\beta \\ -\alpha & -\beta & \alpha^2+\beta^2-\gamma^2 \end{bmatrix}$. After projection transformation, it becomes the ellipse $\boldsymbol{E}=\begin{bmatrix} a & c/2 & d/2 \\ c/2 & b & e/2 \\ d/2 & e/2 & 1 \end{bmatrix}$. The formula is given by

$$s\boldsymbol{E}=\boldsymbol{H}^{-\mathrm{T}}\boldsymbol{C}\boldsymbol{H}^{-1}. \tag{14}$$

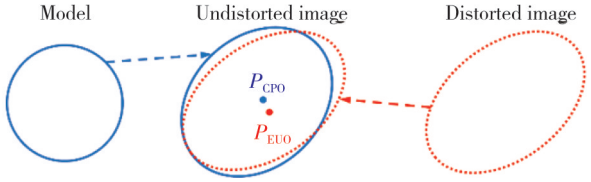

Fig. 3 Illustration of reprojection error

Thus, the coordinates of $\boldsymbol{P}_{\mathrm{CPO}}$ of the ellipse $\boldsymbol{E}$ (Represented by the blue part) can be expressed as $\left(\frac{ce-2bd}{4ad-c^2},\frac{cd-2ae}{4ad-c^2}\right)^{\mathrm{T}}$. Consequently, the reprojection error $\boldsymbol{E}_{\mathrm{RP}}$ can be written as

$$\boldsymbol{E}_{\mathrm{RP}}=\boldsymbol{P}_{\mathrm{EUO}}-\boldsymbol{P}_{\mathrm{CPO}}. \tag{15}$$

After iterative optimization, the optimal $\boldsymbol{O}_{\mathrm{d}}$, λ_1, λ_2, and $\boldsymbol{H}_{(i)}$ are obtained, where the homography matrix is $\boldsymbol{H}_{(i)}=[\boldsymbol{h}_{1(i)}\ \ \boldsymbol{h}_{2(i)}\ \ \boldsymbol{h}_{3(i)}]$. Utilizing the orthogonality constraint of the intrinsic parameter matrix, there is

$$\begin{cases} \boldsymbol{h}_{1(i)}^{\mathrm{T}}\boldsymbol{A}^{-\mathrm{T}}\boldsymbol{A}^{-1}\boldsymbol{h}_{2(i)}=0, \\ \boldsymbol{h}_{1(i)}^{\mathrm{T}}\boldsymbol{A}^{-\mathrm{T}}\boldsymbol{A}^{-1}\boldsymbol{h}_{1(i)}=\boldsymbol{h}_{2(i)}^{\mathrm{T}}\boldsymbol{A}^{-\mathrm{T}}\boldsymbol{A}^{-1}\boldsymbol{h}_{2(i)}, \end{cases} \tag{16}$$

where i represents the ith image. When $i>3$, the camera parameters $\boldsymbol{A}$, $\boldsymbol{R}_{(i)}$, and $\boldsymbol{T}_{(i)}$ can be decomposed. Levenberg-Marquardt (L-M) algorithm minimizes the reprojection error, thereby optimizing the camera parameters. The formula is

$$F(\boldsymbol{A},\boldsymbol{R}_{(i)},\boldsymbol{T}_{(i)})=\min\sum_{i=1}^{m}\sum_{j=1}^{n}\|\boldsymbol{E}_{\mathrm{RP}}\|^2. \tag{17}$$

2.4 Calibration process

Fig.4 presents the stepwise camera calibration process incorporating compensation for the eccentricity error of the circle. The process consists of the five steps.

1) Extract the coordinates of the circle center point, denoted as $\boldsymbol{P}_{d(i,j)}$, from the images. The world coordinates of the model are $\boldsymbol{P}_{w(i,j)}$. Compute the radial distortion fundamental matrix $\boldsymbol{F}_{r(i)}$ for each image based on the point correspondence, and then jointly determine the $\boldsymbol{O}_{\mathrm{d}}$.

2) Optimize $\hat{\boldsymbol{F}}_{r(i)}$ using the proposed Eq. (7). Subsequently, calculate $\lambda_{1(i)}$, $\lambda_{2(i)}$, and $\boldsymbol{H}_{(i)}$, and determine the mean values $\bar{\lambda}_1$ and $\bar{\lambda}_2$.

3) Compute the eccentricity error value $\delta_{(i,j)}$ and compensate for the circle center error using Eq. (13).

4) Repeat steps (1) — (3) until one of the conditions specified in Section 2.2 is satisfied. Upon convergence, calculate the optimal $\boldsymbol{O}_{\mathrm{d}}$, λ_1, λ_2, and $\boldsymbol{H}_{(i)}$.

5) Decompose $\boldsymbol{H}_{(i)}$ to obtain $\boldsymbol{A}$, $\boldsymbol{R}_{(i)}$, and $\boldsymbol{T}_{(i)}$. Subsequently, apply the L-M algorithm to minimize the reprojection error, as described in Eq. (17), in order to optimize these parameters and thus complete the camera calibration process.

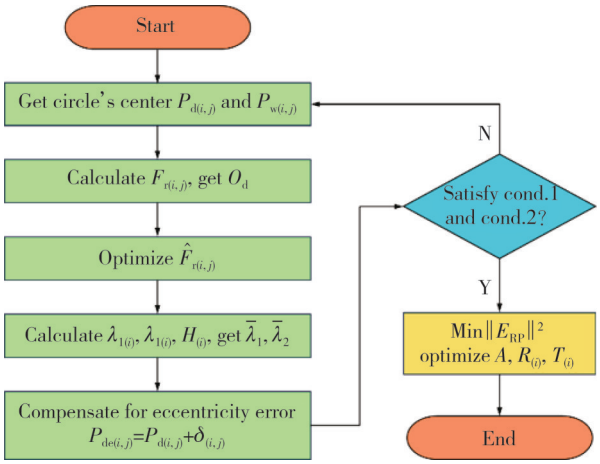

Fig. 4 Illustration of stepwise camera calibration process

3 Simulation and experiment

To evaluate the efficacy of the proposed method, simulations and experiments were conducted by using several relevant camera calibration methods. By comparing the errors of camera parameters under varying noise conditions and utilizing reprojection errors from test data to assess calibration precision, we aimed to comprehensively evaluate these methods.

For the method utilizing the DM model, Hong et al.[22] calculated distortion parameters and the homography matrix through point correspondences, and averaged the results from individual images to determine the final camera calibration outcome. In contrast, Dang et al.[24] calculatedd the common CoD from multiple images and used three projection invariants as constraints for nonlinear optimization to obtain distortion parameters, followed by linear computation of camera parameters. Notably, this method does not provide initial values for distortion coefficients, so we used the order of magnitude of these coefficients as initial values for iterative optimization.

Furthermore, Zhang's method[10], as one of the most commonly used camera calibration methods, is necessary for comparison. Additionally, Shen et al.[18] performed eccentricity error compensation based on Zhang's method. Since both Zhang's[24] and Shen's[18] methods use polynomial models and optimize all parameters simultaneously without addressing the differences between CoD and PP locations,

comparisons are made only for the common aspects.

To validate the efficacy of the multi-image distortion correction method proposed in Section 2.1, we applied it for distortion correction without considering the eccentricity error of the circle compensation and camera parameter optimization, followed by linear camera parameter estimation. This method, referred to as proposed-line due to its linear computation, serves as a basis for comparison with the methods of Hong[22] and Dang[24]. It is important to note that proposed-line is not a complete camera calibration method but it is used solely for comparison purposes. In practical scenarios, compensation for the eccentricity error of the circle and optimization of camera parameters are often necessary. Therefore, the proposed complete camera calibration method is denoted as proposed-Opt, with its principles outlined in Section 2.4, and it is compared with other methods.

To more thoroughly investigate the impact of eccentricity error compensation and camera parameter optimization on calibration results, two additional methods were introduced based on proposed-line. The first method incorporated eccentricity error compensation (Section 2.2) and was termed proposed-COC (Center offset compensation). The second method included nonlinear camera parameter optimization (Section 2.3) and was referred to as proposed-OCP (Optimizing camera parameters). These methods are compared with both proposed-line and proposed-Opt in module comparison experiments to assess the influence of each factor on calibration results.

3.1 Computer simulation

The specifications of the directional array circular target are 9×9 circles, with a large circle radius of 9 mm, a small circle radius of 6 mm, and a center-to-center distance of 18 mm. The simulated camera has an image resolution of 2 448×2 048 pixels, with scaling factors f_x=3 600 and f_y=3 600. The PP and CoD are aligned at (1 224, 1 024). The lens distortion parameters are set to $\lambda_1=-5.0\times10^{-9}$ pixel^{-2} and $\lambda_2=5.0\times10^{-16}$ pixel^{-4}. The target is positioned approximately 300 mm from the camera and rotated within ±45° along the camera axis. A total of 40 simulated target images with varying positions and angles were randomly captured, with 20 images designated for calibration data and the remaining 20 used for test data. The center and contour features of the circles were extracted. Some simulated images are shown in Fig.5. Gaussian noise with a mean of 0 and a standard deviation of σ was added to the distortion points.

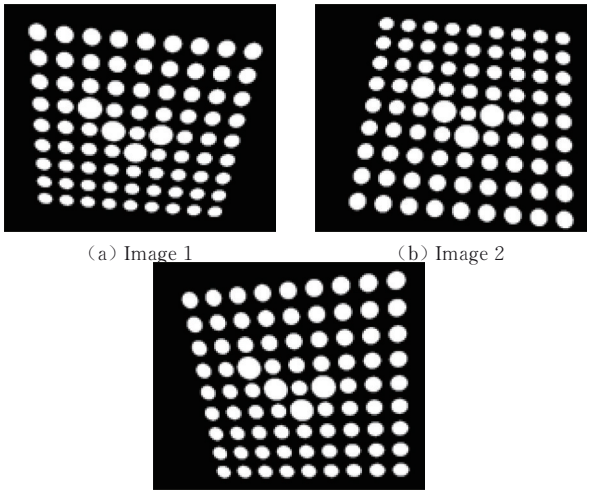

(a) Image 1 (b) Image 2 (c) Image 3

Fig. 5 Sample simulated target images

The estimated distortion parameters are evaluated by comparing them to the true values and calculating the relative errors. Additionally, the re-projection error is assessed using the difference between the circle center projection point measurements $\hat{\boldsymbol{P}}_{\mathrm{COPD},(i,j)}$ and the ideal points $\boldsymbol{P}_{\mathrm{true},(i,j)}$. The mean re-projection error is computed to evaluate calibration precision, as expressed by

$$\boldsymbol{E}_{\mathrm{rms}}=\frac{1}{mn}\sum_{i=1}^{m}\sum_{j=1}^{n}\sqrt{\|\hat{\boldsymbol{P}}_{\mathrm{COPD},(i,j)}-\boldsymbol{P}_{\mathrm{true},(i,j)}\|^2}. \quad (18)$$

This study investigated the impact of various Gaussian noise levels on calibration parameters and $\boldsymbol{E}_{\mathrm{rms}}$. The noise levels range from 0.1 pixels to 2.5 pixels, with a step size of 0.1 pixels. For each noise level, 50 independent experiments were conducted, and the average values were taken as the results for each noise level.

3.1.1 Comparison of distortion correction simulations

Fig.6 illustrates the relative error results of distortion parameters for four methods under various noise levels. All methods utilize the DM model. As noise increases, the relative errors of all distortion parameters gradually increase. Clearly, the proposed-Opt method outperforms the other three methods in terms of relative error of distortion parameters. When the noise level σ=1 (close to natural noise levels), the relative errors of du_0 and dv_0 are both below 3.1%, and the relative errors of λ_1 and λ_2 are below 0.3%. This demonstrates that the proposed-Opt method has better precision and robustness against noise interference.

Compared to the other three methods, Hong's method, which simply averages the calibration results of single images, is more susceptible to noise. At a noise level of σ=1, the relative errors of CoD and distortion coefficients are approximately 5.8% and 15.4%, respectively, indicating lower robustness. The proposed-line method, employing multi-image distortion correction, shows better levels and

variations of relative errors for distortion parameters compared to the previous method. When the noise level is $\sigma=1$, the relative errors of CoD and distortion coefficients are within 5.0% and 8.5%, respectively, proving that the multi-image distortion correction method offers high precision and robustness.

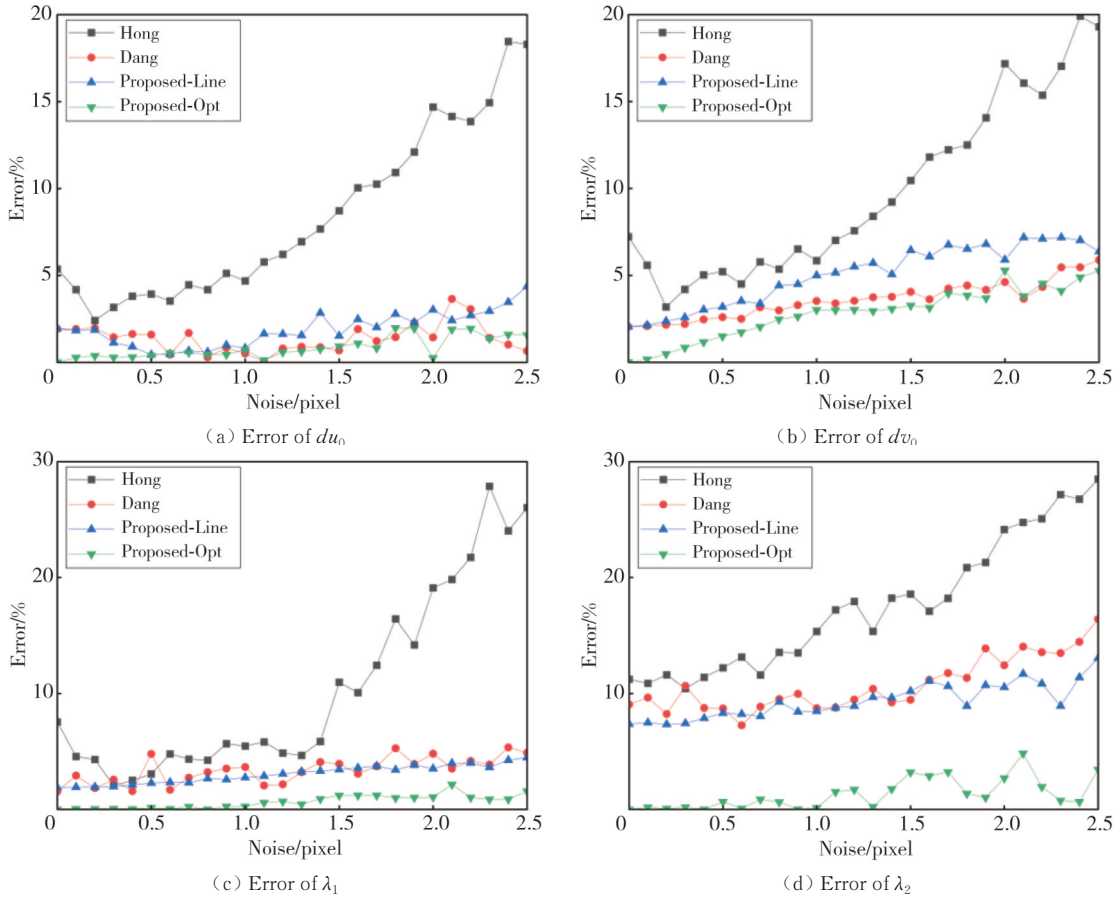

Fig. 6 Relative error of distortion parameters across methods at different noise levels

With the initial values provided in this study, Dang's[24] method yields results similar to those of the proposed-line method. However, Dang's[24] method involves nonlinear iterative computation of distortion coefficients, which can lead to local minima and unstable results. Additionally, nonlinear iterations are more complex and time-consuming. In contrast, the proposed-line method does not require nonlinear iterations and is more efficient.

3.1.2 Comparison of camera calibration simulations

Table 1 presents the simulated calibration results using different methods without noise. It is evident that the parameters obtained using the proposed-Opt method are very close to the true values, with f_x, f_y, λ_1, and λ_2 matching the true values exactly, while other parameters are also close to the true values.

Table 1 Simulated calibration results for different methods without noise

Method	f_x/pixel	f_y/pixel	u_0/pixel	v_0/pixel	du_0/pixel	dv_0/pixel	λ_1/e^{-9} pixel^{-2}	λ_2/e^{-16} pixel^{-4}
Ground truth	3 600	3 600	1 224	1 024	1 224	1 024	−5	5
Hong[22]	3 567.79	3 567.71	1 225.01	1 022	1 289.77	950.02	−4.62	4.44
Dang[24]	3 569.81	3 569.83	1 224.52	1 021.22	1 247.63	1 002.96	−4.92	4.55
Zhang[10]	3 600.22	3 600.21	1 224.17	1 023.96	—	—	—	—
Shen[18]	3 599.98	3 599.98	1 224.04	1 024.05	—	—	—	—
Proposed-Line	3 569.48	3 569.6	1 224.53	1 021.81	1 247.62	1 002.96	−4.91	4.63
Proposed-Opt	3 600	3 600	1 224.03	1 023.98	1 224.17	1 023.86	−5.00	5.00

This demonstrates the high computational precision of the method. Additionally, although Zhang's[10] and Shen's[18] methods use different parameter models, the camera parameters from both methods show relatively small errors. This indicates that full-parameter iterative optimization can achieve high computational precision to some extent, and Shen's[18] method, which compensates for the eccentricity error of the circle, provides calibration results closer to the true values. A detailed examination of Shen's[18] camera parameters reveals that compared to the proposed-Opt method, Shen's method[18] exhibits relatively larger errors. This suggests that Shen's[18] full-parameter

optimization camera calibration method may produce overfitting errors, leading to locally optimal solutions in the presence of parameter errors, thereby proving that stepwise camera calibration has higher robustness.

In contrast, the calibration results of the proposed-line method are closer to the true values than those of Hong's[22] method, further demonstrating the superior precision of the proposed multi-image distortion correction method. The proposed-line method yields results similar to those of Dang's[24] method. Both methods compute the CoD using the same principles, with the former employing linear distortion coefficient solutions and the latter using nonlinear optimization. This comparison confirms that, although the precision of the former method is similar to that of the latter, it has higher computational efficiency.

To evaluate the calibration results of different methods more clearly, the average reprojection error for 20 test images are calculated under varying noise levels, as shown in Fig.7.

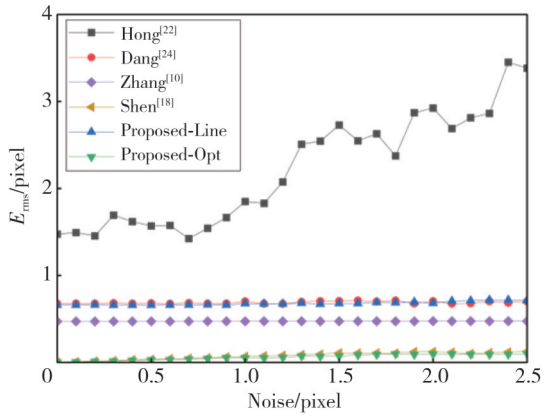

Fig. 7 Average reprojection errors for different methods at various noise levels

It is evident that the proposed-Opt method achieves the lowest average re-projection error compared to other methods, demonstrating that the calibration method outlined in Section 2.4 results in high precision and enhanced robustness. In conjunction with Fig. 8, with error bars indicating the standard deviation, when the noise level $\sigma=1$ (close to natural noise levels), the proposed-Opt method achieves higher precision with a re-projection error of only 0.050 pixels. This error is 26.47% lower than that of Shen's method, highlighting the greater robustness and improved precision of the stepwise camera calibration method. Compared to the traditional Zhang's[10] method, which does not account for the eccentricity error of the circle, the proposed-Opt method reduces the re-projection error by 89.41%. The smaller standard deviation indicated by the error bars further supports that compensating for the eccentricity error of the circle results in high precision and enhanced stability. Among the three methods discussed, all of which utilize nonlinear optimization for calibration parameters, the re-projection errors are lower than those of other methods, indicating that nonlinear optimization contributes to higher calibration precision.

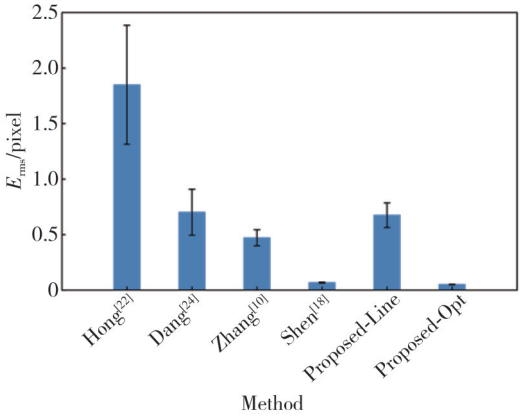

Fig. 8 Test errors for different methods when σ=1

When $\sigma=1$, the proposed-line method reduces the reprojection error by 63.5% compared to the Hong's[22] method, demonstrating high precision in multi-image distortion correction. The reprojection error of the proposed-line method is similar to that of the Dang's[24] method, but the standard deviation is 46.38% lower, indicating that the proposed-line method achieves a nonlinear level of distortion correction through linear computation, providing both high efficiency and greater stability.

In summary, the proposed-Opt method offers improved robustness and precision compared to the Shen's[18] method, demonstrating that stepwise camera calibration is more robust than full-parameter optimization methods. The proposed-Opt method shows high precision and more stable results than the Zhang's[10] method, highlighting the critical importance of compensating for the eccentricity error of the circle in camera calibration. The proposed-Opt method incorporates both bias compensation and nonlinear optimization, resulting in significantly better outcomes than the proposed-line method. The proposed-line method outperforms the Hong's[22] method in precision, and surpasses the Dang's[24] method in stability and computational efficiency, proving that the proposed multi-image distortion correction algorithm achieves superior precision, stability, and computational efficiency.

3.1.3 Comparison of camera calibration module simulations

To further investigate the impact of compensating for the eccentricity error of the circle and optimizing camera parameters on camera calibration results, a series of module comparison experiments were conducted.

Table 2 presents the relative errors of the simulated results for different methods when σ=1.

Table 2 Relative errors of simulated results for different methods when σ=1

Method	E_{fx}/%	E_{fy}/%	E_{u0}/%	E_{v0}/%	E_{du0}/%	E_{dv0}/%	E_{λ_1}/%	E_{λ_2}/%
Proposed-Line	0.85	0.85	0.22	0.50	0.82	5.00	2.80	8.40
Proposed-COC	0.04	0.05	0.09	0.09	0.35	2.89	0.33	0.38
Proposed-OCP	0.03	0.03	0.04	0.49	0.70	3.57	1.67	6.08
Proposed-Opt	0.00	0.00	0.04	0.39	0.32	2.94	0.34	0.36

Test errors for proposed different methods when σ=1 are shown as Fig.9.

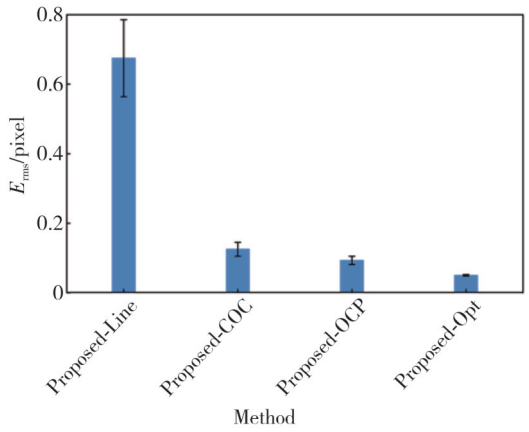

Fig. 9 Test errors for proposed different methods when σ=1

Combining with Fig. 9, the proposed-line method, which does not account for the eccentricity error of the circle or camera parameter optimization, exhibits very large relative errors, with the maximum λ_2 being 8.40%. The proposed-COC method, which incorporates compensation for the CoD, demonstrates a lower relative error in distortion parameters compared to the proposed-line and proposed-OCP methods. The reprojection error for this method is 0.125 pixels, which is 81.48% less than that of the proposed-line method, indicating that compensating for the eccentricity error of the circle improves result precision. The proposed-OCP method shows lower relative errors in camera parameters and a smaller average reprojection error compared to both the proposed-line and proposed-COC methods, with an average reprojection error of 0.093 pixels, reduced by 86.22% compared to the proposed-line method. It underscores the importance of camera parameter optimization following distortion correction. Additionally, this method outperforms the proposed-COC method in terms of reprojection error and standard deviation, suggesting that nonlinear optimization can significantly enhance calibration results compared to eccentricity error compensation, though the latter should not be disregarded. The proposed-Opt method, which integrates both compensation for the eccentricity error of the circle and camera parameter optimization, achieves the smallest average reprojection error and standard deviation at 0.050 pixels and 0.002 pixels, respectively, demonstrating its superior precision and robustness.

3.2 Real experiment

The used camera was the Basler aceU-acA2440-35 um with a resolution of 2 448 × 2 048 pixels and a pixel size of 3.45 μm. The lens employed was the Basler C23-1616-2M-S with a focal length of 12 mm and a working distance of approximately 300 mm. The used target was the same as described in the simulation experiments, featuring a directional array of circular targets. The targets were evenly placed at different positions within the camera's field of view, capturing 20 images for camera calibration, followed by another 20 images as test data to evaluate the calibration results. The physical image of camera calibration is shown in Fig.10.

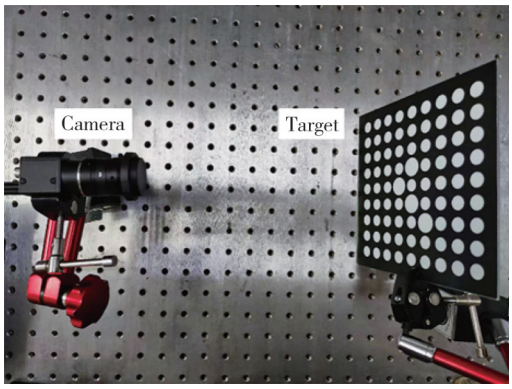

Fig. 10 Physical image of camera calibration

In the experiment, the acquired test target images were preprocessed. Subpixel detection methods[27] were used to obtain the circular contours, and least-squares fitting was applied to determine the coordinates of the circle's center. To compensate for the eccentricity error of the circle and precision evaluate the camera calibration results, the average re-projection error is calculated using Eq. (15) from Section 2.3. The formula for calculating the average re-projection error is

$$E'_{\mathrm{rms}}=\frac{1}{mn}\sum_{i=1}^{m}\sum_{j=1}^{n}\sqrt{\|\boldsymbol{P}_{\mathrm{EUO},(i,j)}-\boldsymbol{P}_{\mathrm{CPO},(i,j)}\|^2}\,. \quad (19)$$

3.2.1 Comparison of camera calibration experiments

Table 3 presents the calibration results for different methods. It is evident that the calibration parameters for

Shen's[18] and proposed-Opt methods are similar, indicating that the proposed-Opt method achieves a level of performance comparable to Shen's[18] method in practical camera calibration.

Table 3 Calibration results for different methods

Method	f_x/pixel	f_y/pixel	u_0/pixel	v_0/pixel	du_0/pixel	dv_0/pixel	λ_1	λ_2
Hong[22]	3 590.49	3 589.59	1 236.80	982.35	1 226.71	958.16	$-5.58e^{-9}$ pixel^{-2}	$5.48e^{-16}$ pixel^{-4}
Dang[24]	3 559.97	3 559.79	1 237.81	981.99	1 215.90	970.48	$-5.38e^{-9}$ pixel^{-2}	$4.92e^{-16}$ pixel^{-4}
Zhang[10]	3 597.25	3 597.05	1 241.06	980.68	—	—	-0.073 mm^{-2}	0.10 mm^{-4}
Shen[18]	3 613.67	3 613.32	1 240.90	980.29	—	—	-0.0741 mm^{-2}	0.10 mm^{-4}
Proposed-Line	3 544.54	3 544.04	1 236.69	980.27	1 215.90	970.48	$-5.64e^{-9}$ pixel^{-2}	$5.60e^{-16}$ pixel^{-4}
Proposed-Opt	3 609.70	3 609.42	1 239.97	983.89	1 215.47	965.65	$-5.71e^{-9}$ pixel^{-2}	$5.79e^{-16}$ pixel^{-4}

To evaluate the calibration results of different methods, 20 images were used as test data. As shown in Fig. 11, the test errors obtained using various methods are presented, with error bars indicating the standard deviation.

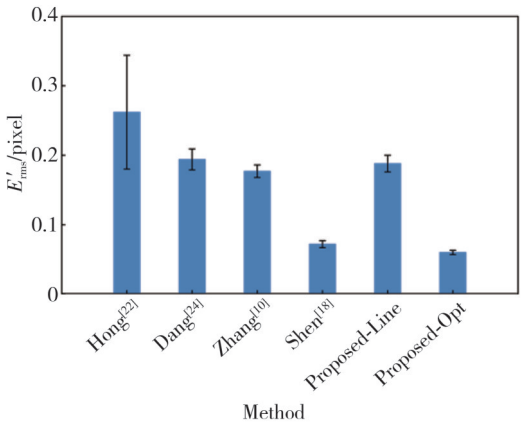

Fig. 11 Test errors for different methods

Fig. 12 shows the feature point errors for different methods. Consistent with the simulation experiment conclusions, the eccentricity error compensation incorporated into Shen's[18] method and the proposed-Opt method results in low reprojection errors, specifically 0.072 pixels and 0.060 pixels, respectively. The reprojection error of the proposed-Opt method is 16.67% lower than that of Shen's[18] method, indicating high calibration precision. However, as observed in Fig.12(d) and 12(f), feature point errors from Shen's[18] method are more dispersed and affected by noise or outliers, demonstrating that stepwise camera calibration yields higher precision and robustness compared to full parameter optimization methods. The proposed-Opt method reduces the reprojection error by 66.10% and the standard deviation by 66.67% compared to Zhang's[10] method, confirming that compensation for the eccentricity error of the circle enhances both calibration precision and stability. All three methods outperform other methods in terms of reprojection error, indicating that nonlinear optimization of calibration parameters generally leads to higher precision in calibration results.

As seen in Fig.11, the reprojection error and standard deviation of the proposed-line method are better than those of Hong's method and comparable to Dang's[24] method, suggesting higher precision. The proposed-line method achieves performance equivalent to Dang's[24] nonlinear optimization through linear computations, indicating higher computational efficiency. Additionally, Fig.12(a), 12(b), and 12(e) demonstrate that feature point errors for the proposed-line method are more concentrated compared to Hong's[22] and Dang's[24] methods, suggesting greater stability. This evidence supports that the multi-image distortion correction method proposed in Section 2.1 offers improved precision, robustness, and computational efficiency.

3.2.2 Comparison for camera calibration module experiments

Fig.13 shows the test errors for the different proposed methods. The proposed-COC and proposed-OCP methods, which individually address the compensation for the eccentricity error of the circle and camera parameter optimization, demonstrate a reduction in average reprojection error of 56.91% and 57.98%, respectively, compared to the proposed-line method. It indicates the efficacy of these algorithms in improving camera calibration. The proposed-OCP method yields slightly better results than the proposed-COC method, suggesting that nonlinear optimization of camera parameters has a more significant impact on the results, while compensation for the eccentricity error of the circle also plays an important role.

Undoubtedly, the proposed-Opt method achieves superior calibration precision and robustness due to its simultaneous compensation for the eccentricity error of the circle and optimization of camera parameters. Among the methods evaluated, it reduces the reprojection error and standard deviation more significantly, with reductions of 68.09% and 75.00%, respectively, compared to the proposed-line method.

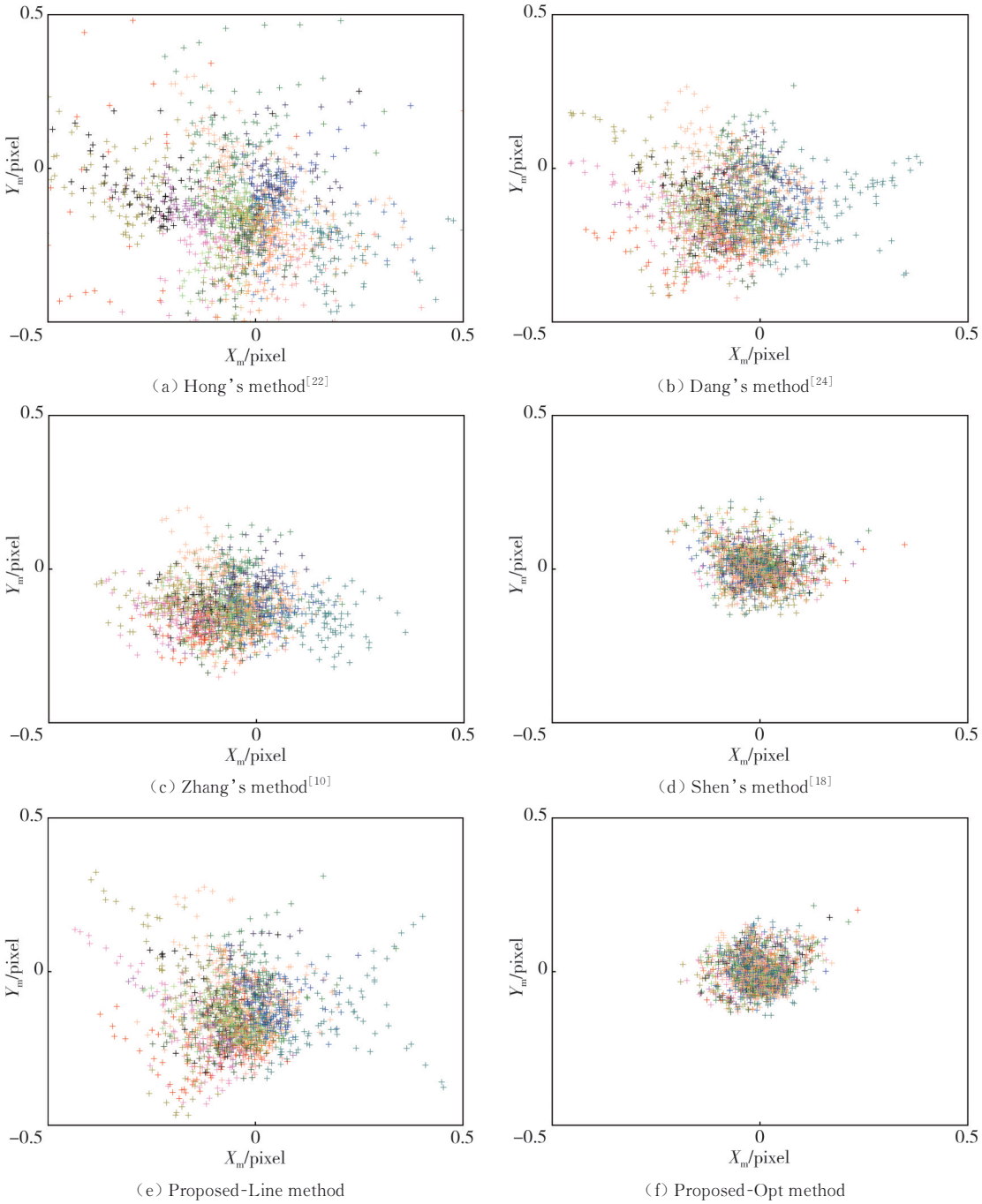

Fig. 12 Feature point errors for different methods

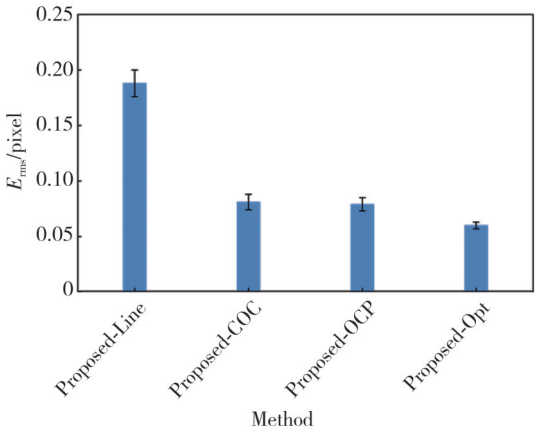

Fig. 13 Test errors for different proposed methods

4 Conclusions

A stepwise camera calibration method was proposed that incorporated compensation for the eccentricity error of the circle. Firstly, a multi-image distortion correction method was introduced, which accounted for the position of the CoD and coefficients, enhancing the precision, stability, and computational efficiency of the distortion correction. Moreover, the method iteratively compensated for the eccentricity error of the circle, leading to improved calibration precision and stability. Finally, stepwise calibration of distortion parameters

and camera parameters was achieved, avoiding excessive model parameters that could lead to overfitting errors or local optima, thereby increasing the robustness of the calibration results. Furthermore, the impact of compensating for the eccentricity error of the circle and the nonlinear optimization of camera parameters was investigated on camera calibration. Experimental results demonstrated that both factors positively influenced camera calibration, with the latter having a more significant effect. When both methods were applied simultaneously, the precision and stability of camera calibration were further enhanced. Results from both simulated and real experiments validated the proposed method's superior precision, stability, and robustness. In real experiments, the proposed method demonstrated a reduction in reprojection error of 66.10% and 16.67% compared to the traditional methods introduced by Zhang and Shen, respectively. This significant improvement highlighted the method's superiority, making it suitable for applications in high-precision visual measurement fields.

Declaration of conflicting interests

The authors have no conflict of interests related to this publication.

References

[1] QIAN S W, LIANG J Z, LIANG J, et al. Hybrid calibration method for a single camera stereo digital image correlation system. Applied Optics, 2024, 63(19): 5099.

[2] ZHENG Z, FAN J F, SHAO L, et al. Affine constrained binocular camera calibration with planar target single-axis translating. IEEE Transactions on Instrumentation and Measurement, 2024, 73: 5018313.

[3] HUANG J C, LIU S L, LIU J H, et al. Camera calibration optimization algorithm that uses a step function. Optics Express, 2024, 32(11): 18453-18471.

[4] YIN Y L, ZHU H B, YANG P, et al. Robust and accuracy calibration method for a binocular camera using a coding planar target. Optics Express, 2022, 30(4): 6107-6128.

[5] ZHANG X W, LV T G, DAN W, et al. High-precision binocular camera calibration method based on a 3D calibration object. Applied Optics, 2024, 63(10): 2667-2682.

[6] GUAN B L, YU Y J, SU A, et al. Self-calibration approach to stereo cameras with radial distortion based on epipolar constraint. Applied Optics, 2019, 58(31): 8511-8521.

[7] CHANG D X, HUANG S J, ZHOU Y S, et al. Target-free stereo camera-GNSS/IMU self-calibration based on iterative refinement. IEEE Sensors Journal, 2023, 24(3): 3722-3730.

[8] WANG Y, WANG X J. On-line three-dimensional coordinate measurement of dynamic binocular stereo vision based on rotating camera in large FOV. Optics Express, 2021, 29(4): 4986-5005.

[9] YU B C, ZHANG Y Z, LIU W, et al. A robotic spindle end high- accuracy positioning method based on eye-in-hand vision active correction. IEEE Transactions on Instrumentation and Measurement, 2023, 72: 5024011.

[10] ZHANG Z. A flexible new technique for camera calibration. IEEE Transactions on Pattern Analysis and Machine Intelligence, 2002, 22(11): 1330-1334.

[11] DATTA A, KIM J S, KANADE T. Accurate camera calibration using iterative refinement of control points// 2009 IEEE 12th International Conference on Computer Vision Workshops, ICCV Workshops, September 27-October 4, 2009, Kyoto, Japan. New York: IEEE, 2009: 1201-1208.

[12] YANG L M, ZHOU F Q, ZHANG W N, et al. A novel camera calibration method based on circle projection model. Measurement, 2023, 222: 113651.

[13] YU Z Y, SHEN G T, ZHAO Z Y, et al. An out-of-focus image calibration method based on accurate positioning of concentric circle projection center. IEEE Access, 2023, 11: 69216-69226.

[14] YU J, LIU Y, ZHANG Z H, et al. High-accuracy camera calibration method based on coded concentric ring center extraction. Optics Express, 2022, 30(23): 42454-42469.

[15] WEN G, YANG Y F, YANG Z Y, et al. A high-accuracy camera calibration method based on special circular target//2022 International Conference on Industrial Automation, Robotics and Control Engineering, June 10-12, 2022, Chengdu, China. New York: IEEE, 2022: 24-28.

[16] LIANG S X, ZHAO Y. Camera calibration based on the common pole-polar properties between two coplanar circles with various positions. Applied Optics, 2020, 59(17): 5167-5178.

[17] LIN X D, ZHANG X. Accurate camera calibration method based on perspective distortion correction. Laser & Optoelectronics Progress, 2023, 60(16): 3788.

[18] SHEN Y J, ZHANG X, CHENG W, et al. Quasi-eccentricity error modeling and compensation in vision metrology. Measurement Science and Technology, 2018, 29(4): 045006.

[19] RICOLFE-VIALA C, SANCHEZ-SALMERON A J, VALERA A. Efficient lens distortion correction for decoupling in calibration of wide angle lens cameras. IEEE Sensors Journal, 2012, 13(2): 854-863.

[20] FANG W, ZHENG L Y. Distortion correction modeling method for zoom lens cameras with bundle adjustment. Journal of the Optical Society of Korea, 2016, 20(1): 140-149.

[21] HARTLEY R I, KANG S B. Parameter-free radial distortion correction with centre of distortion estimation//

Tenth IEEE International Conference on Computer Vision (ICCV′05) Volume 1, October 17-21, 2005, Beijing, China. New York: IEEE, 2005: 1834-1841.

[22] HONG Y Z, REN G Q, LIU E H. Non-iterative method for camera calibration. Optics Express, 2015, 23(18): 23992-24003.

[23] SUN L J, GUO Q Q, CHEN T F, et al. Non-metric correction method for complete lens distortion using dual-characteristics joint measurement. Optical Engineering, 2022, 61(7): 074101.

[24] DANG Z Y, ZHANG Z Y, WANG Z H. Camera field calibration method using collinear point target joint constraints//2023 9th International Conference on Virtual Reality, May 12-14, 2023, Xianyang, China. New York: IEEE, 2023: 115-122.

[25] BROWN D. Close-range camera calibration. Photogrammetric Engineering. 1971, 37(8): 855-866.

[26] FITZGIBBON A. Simultaneous linear estimation of multiple view geometry and lens distortion//2001 IEEE Computer Society Conference on Computer Vision and Pattern Recognition, December 08-14, 2001, Kauai, HI, USA. New York: IEEE, 2001: 990465.

[27] LI Q L, ZHANG S J, LI Z F, et al. A improved subpixel edge detecting algorithm based on polynomial interpolation. Chinese Journal of Engineering, 2003, 25(3): 280-283.

考虑圆心偏差补偿的分步相机标定方法

魏家起，王　鹏*，李　岳，李默晶，李　林，孙长库，付鲁华

天津大学 精密测试技术及仪器全国重点实验室，天津 300072

摘　要：在视觉测量领域，高精度的相机标定往往采用圆形目标。为了解决主流相机标定算法使用圆心标定造成圆心偏差、使用全参数优化产生过拟合或容易陷入局部最优解、以及忽略畸变中心产生标定误差的问题，本文提出了一种考虑圆心偏差补偿的分步相机标定方法，用于实现单目相机的高精度标定。首先，与传统的单图像畸变校正方法不同，本文提出的多图像畸变校正方法可以计算共同的畸变中心和系数，使畸变校正精度更高，稳定性和计算效率更强；其次，将圆心投影点与圆轮廓投影中心的差值作为圆心偏差进行补偿，重复迭代上述过程，使标定结果精度更高更稳定；最后，通过最小化重投影误差对相机参数非线性优化，完成畸变参数和相机参数的分步式标定，进一步提高了标定结果的鲁棒性。另外，本文通过模块对比实验研究了圆心偏差补偿和相机参数优化对相机标定的影响，结果表明两者都可提升标定精度，且后者作用更大，当两者同时使用时标定精度和稳定性进一步得到提高。本文进行了计算机仿真和真实实验，均证明了本文所提方法具有较高的精度、较强的稳定性和鲁棒性，可用于高精度的视觉测量领域。

关键词：相机标定；圆心偏差；误差补偿；畸变校正；畸变中心；光学测量

引用格式：WEI Jiaqi, WANG Peng, LI Yue, et al. A stepwise camera calibration method incorporating compensation for eccentricity error. Journal of Measurement Science and Instrumentation, 2024, 15(4): 445-457.